Shedding light on active species in Fe, Ni and Cu catalysis

Draksharapu, Apparao

Chapter 7

Spectroscopic characterisation of Ni^{II}-$O^{\cdot}$ species in the reaction of a non-porphyrinic Ni(II) complex with NaOCl

In this chapter, the characterisation of a non-porphyrinic $Ni^{II}(^{H,Me}PyTACN)$ complex and its reactivity with NaOCl by UV/Vis absorption, (resonance)Raman, ^{1}H NMR and EPR spectroscopy, cyclic voltammetry and ESI-MS is reported. Evidence for a Ni^{II}-$O^{\cdot}$ species as well as a Ni^{II}-OCl complex is presented together with the selective and efficient catalytic chlorination of alkanes with NaOCl catalysed by the complex.

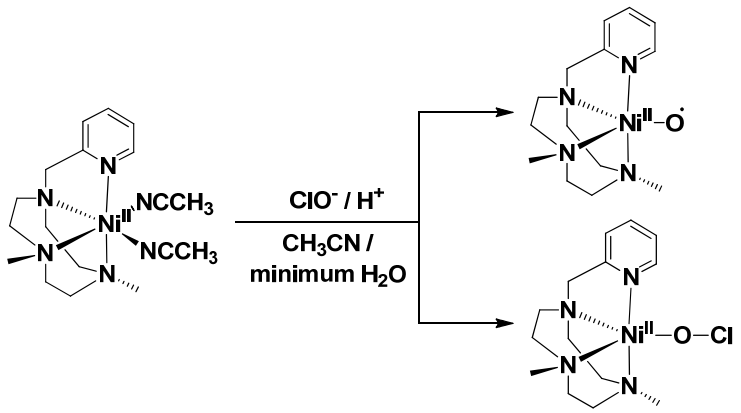

A. Draksharapu, D. Angelone, A. Company, Z. Codolà, J. Lloret-Fillol, L. Gómez, W. R. Browne, M. Costas, *to be submitted.*

7.1 Introduction

Metal catalysed oxidations play a central role in a myriad of biological and chemical processes as discussed in the preceding chapters.[1] These reactions typically involve the formation of highly reactive inorganic (transition metal) species, where the terminal oxidant acts in the first instance as a ligand.[2] Subsequent oxidation of the metal concomitant with formation of a terminally bound oxo ligand occurs frequently.[3] The most prominent examples are the metal-peroxides and hydroperoxides, however, other classes of metal-oxidant complexes have been proposed in recent years and are gaining interest, due to the increasing number of direct structural, spectroscopic and reactivity studies of enzymatic systems.[4] Important examples include non-porphyrinic iron and manganese complexes ligated to iodosylbenzenes,[5] for which X-ray structures have been determined, and a single example of a Heme Fe^{III}-OCl intermediate was described recently.[6] Investigation of the chemistry of these highly reactive species is challenging due to their inherent instability, however, valuable insight relevant to a wide range of biological oxidative transformations can be gained through such studies.

The direct conversion of an aliphatic C-H bond to a C-Cl bond is an important and challenging goal in transition metal based oxidation catalysis both for synthetic applications and to understand the mechanisms by which metalloenzymes, in particular, haloperoxidases operate.[7] Over the past decades, numerous metal catalysed C-H activation reactions have been developed for directed oxygenation.[8] The hypochlorite anion constitutes a versatile oxidant that has found wide spread application in metal catalysed oxidations employed in organic synthesis.[9] Several manganese, iron and nickel catalysed oxidations are based on the use of NaOCl, however, to date, to the best of our knowledge, evidence for M-OCl species (M = Mn, Fe, Ni) has not been reported in any non-porphyrinic systems and only one example has been described for a heme system recently by Fujii *et al* (notwithstanding chapter 6, of course).[6]

Catalytic halogenation of non-activated alkyl C-H groups, although receiving much less attention, has been achieved also, for example, with manganese porphyrin catalysts and sodium hypochlorite; the latter acting both as oxidant and source of the halogen atom to be incorporated.[9b] Ni-salen complexes and indeed Ni(II) salts have been shown to be capable of oxidative chlorination also, albeit requiring a gross excess (40 times) of the oxidant NaOCl.[10] It has been proposed in the context

of nickel based catalysis that a nickel oxo species (Ni^{IV}=O or Ni^{III}=O/Ni^{II}-O$^{\cdot}$)[11,12,13] is responsible for catalytic activity of these complexes. Furthermore, a Ni^{III}=O(H)/Ni^{II}-O$^{\cdot}$ active intermediate in catalysis with mCPBA has been proposed by Itoh[12] and Ray,[13] recently. Spectroscopic evidence for these intermediates is, however, not yet available. Moreover, the existence of a Ni^{IV}=O intermediate proposed by Burrows[11] is rather unlikely considering the 'oxo wall' (Fe-Ru-Os), *i.e.* metals to the right of the wall will not support a terminal oxo group in a tetragonal environment.[14,15]

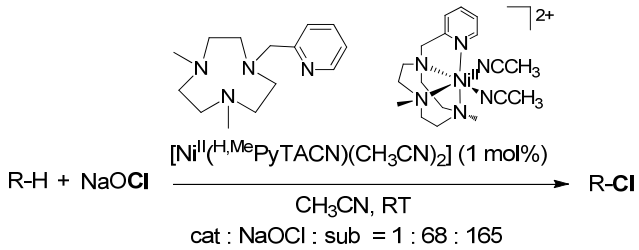

Scheme 1 Structure of the ligand ^{H,Me}PyTACN and its Ni(II) complex and the catalysed halogenation of alkanes with NaOCl.

In this chapter, for the first time the direct spectroscopic characterisation of Ni^{II}-O$^{\cdot}$ and Ni^{II}-OCl species is described. These species are formed as intermediates during the catalytic halogenation of alkanes. The non-porphyrinic complex $[Ni^{II}(^{H,Me}PyTACN)(CH_3CN)_2](OTf)_2$ (**1**) catalyses the halogenation of aliphatic C-H bonds using NaOCl both as terminal oxidant and chlorine source (Scheme 1). UV/Vis absorption, resonance Raman, NMR and EPR spectroscopic data indicate that the active form of the catalyst is Ni^{II}-O$^{\cdot}$ species (C-H abstraction) and Ni^{II}-OCl (chlorinating agent) species. Catalyst **1**, with sodium hypochlorite, transforms a range of alkanes to alkyl chlorides with good selectivity and with only minor amounts of oxygenated and other chlorinated products under optimised conditions. Several aspects of the reactivity of these species in oxygen atom transfer reactions are described also.

7.2 Results and discussion

7.2.1 Synthesis and Characterisation of 1

The ligand ^{H,Me}PyTACN was available from earlier studies.[16] Complex **1** was prepared by reaction of equimolar amounts of the ligand ^{H,Me}PyTACN and $[Ni^{II}(CH_3CN)_6](OTf)_2$ in acetonitrile and isolated as pale violet crystals. The UV/Vis absorption spectrum of **1** in acetonitrile shows λ_{max} at 275, 321, 525, 809

and 906 nm (*vide infra,* Figure 4a). The spectrum is similar to that of $[Ni^{II}(TPA)(OAc)(H_2O)](BPh_4)$.[17] By analogy, the bands in the UV region are assigned to intra-ligand transitions, and the bands at 525 and 906 nm are assigned to $^3A_{2g} \rightarrow {}^3T_{1g}$ (F) and $^3A_{2g} \rightarrow {}^3T_{2g}$ (F) transitions, respectively. The band at ca. 809 nm is assigned tentatively, as a spin forbidden $^3A_{2g} \rightarrow {}^1E_{1g}$ transition.[17,18]

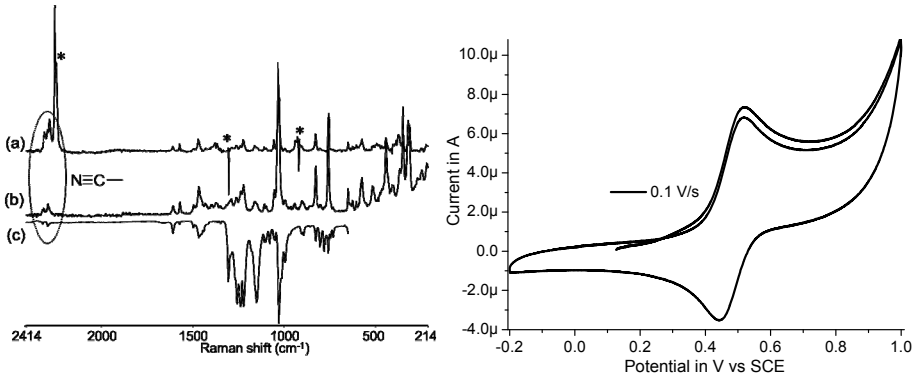

Figure 1 (left) Raman spectra of **1** (a) 75 mM in acetonitrile (solvent subtracted) (b) as a solid powder λ_{exc} 785 nm and (c) FTIR spectrum and (right) cyclic voltammetry of **1** (1 mM) in acetonitrile (10 mM TBAP, *vs.* SCE). * artefact from solvent subtraction.

The cyclic voltammetry of **1** in acetonitrile shows a single quasi-reversible redox wave for the Ni^{III}/Ni^{II} redox couple at 0.48 V *vs.* SCE (Figure 1). The coordination of acetonitrile ligands both in solution and the solid state is apparent from the nitrile bands of **1** at 2293 cm^{-1} and 2318 cm^{-1} in both the FTIR and Raman spectra. The Raman spectra recorded under non-resonant conditions at λ_{exc} 785 nm of both crystalline material and a 75 mM solution in acetonitrile of **1** are (with the exception of solvent bands) identical both in terms of Raman shift and relative intensity of the modes (Figure 1). The nitrile stretching bands of the CH_3CN ligand of **1** in the solid state at 2293 cm^{-1} and 2318 cm^{-1}, are observed at the same wavenumbers in solution also. The close correlation between FTIR and Raman spectra of **1** in the solid state with the non-resonant Raman spectrum in acetonitrile confirms that the structure of complex **1**, *i.e.* the tetradentate coordination of the PyTACN ligand to the Ni^{II} centre, is retained in solution.

Crystals suitable for X-ray crystallographic analysis were obtained by slow diffusion of diethyl ether into an acetonitrile solution of **1**. Complex **1** adopts a distorted octahedral geometry with six nitrogen donors (Figure 2). Four coordination sites are occupied by N atoms from the ligand PyTACN and the other two by acetonitrile. The acetonitrile ligands are *cis* to each other. The six Ni-N

bonds range from 2.046 to 2.112 Å and are similar to those reported for the complex $[Ni^{II}(TPA)(OAc)(H_2O)](BPh_4)$.[12]

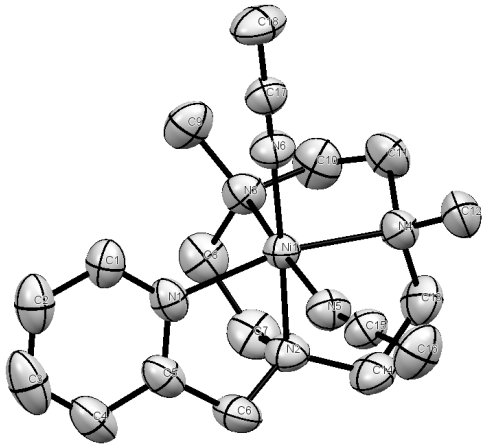

	Bond length (in Å)
Ni-N1$_{py}$	2.079 (3)
Ni-N2$_{amine}$	2.061 (3)
Ni-N3$_{amine}$	2.112 (3)
Ni-N4$_{amine}$	2.105 (3)
Ni-N5$_{acn}$	2.105 (3)
Ni-N6$_{acn}$	2.046 (3)

Figure 2 Structure of **1** with 50% probability ellipsoids along with the bond distances. Hydrogen atoms and triflate anions are removed for clarity.

7.2.2 Catalytic C-H activation with 1 and NaOCl

The oxidation of alkanes with sodium hypochlorite, catalysed by **1** (1 mol%, 1 mg scale), is summarised in Table 1. Conversion was not observed in the absence of **1** or in the presence of $[Ni^{II}(O_2CCH_3)_2]$. Chlorocyclohexane and chlorocyclooctane were obtained in 17% and 12% yield, respectively, with respect to the terminal oxidant and 6% and 4% yield, respectively, with respect to the substrate cyclohexane and cyclooctane. For both substrates the only mono-oxygenated products obtained were the corresponding ketones. In the case of n-hexane (entry 4), the mono chlorinated products 2-chlorohexane and 3-chlorohexane were obtained as the major products. A competition reaction between cyclohexane and cyclohexane-d_{12} yielded a kinetic isotopic effect of 2, consistent with the involvement of a highly reactive hydrogen abstracting reagent.[8b] Notably however, chlorination of adamantane proceeds with high regioselectivity towards chlorination at the tertiary C-H position ($3^o/2^o = 8.6$), which is inconsistent with the involvement of hydroxyl radicals.[19]

Table 1 Oxidative halogenation of aliphatic hydrocarbons

		Without acetic acid[b]			**With acetic acid**[c]		
Substrate[d]	Products	Yield[a] Ox (%)	TON	Comments	Yield[a] Ox (%)	TON	comments
	Chlorocyclohexane Cyclohexanone	17 4	10	C/K = 4.4:1	37 3	25 2	C/K = 14.7:1
	1-chloroadamantane 2-chloroadamantane 1-adamantanol 2-adamantanol + adamantanone	12 4 7 3	13	3°/2° = 8.6:1	37 14 --- ---	25 10 --- ---	3°/2° = 7.7:1
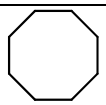	Chlorocyclooctane Cyclooctanone	11 1	6	---	28 6	19 4	C/K = 5:1
	2-chlorohexane 3-chlorohexane	6 6	3 3	traces ketone	11 11	7 7	traces ketone
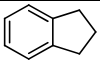	Indanone[e]	---	---	---	36	24	only ketone

[a]Yield based on oxidant, [b]conditions: (**1**/oxidant/substrate) 1:68:165, [c]conditions: (**1**/oxidant/substrate/acetic acid) 1:68:165:27 and [d]in acetonitrile except for adamantane (1:1 CH_2Cl_2 and CH_3CN). All yields were determined by GC except 'e' (NMR yield with dichlorobenzene as internal standard). C and K are Chloro and Ketone products, respectively.

Interestingly, in the presence of up to 27 equivalents of acetic acid the conversion to chlorocyclohexane increased over twofold to 37 and chloro/ketone ratio improved from 4 to 15. The increased conversion to the corresponding chlorinated products in the presence of acetic acid (Table 1) was observed in the case of adamantane and cyclooctane also. In the case of n-hexane conversion to the corresponding chloro products increased twofold. With indane, which has a relatively weak benzylic C-H bond, indanone is the only product observed in 36% yield with respect to the terminal oxidant.

The catalytic oxidation of cyclohexane in the absence of acetic acid was monitored by Raman spectroscopy, with conversion monitored by the decrease in the relative intensity of the cyclohexane band at 804 cm^{-1} with respect to a band of the internal standard 1,2-dichlorobenzene at 662 cm^{-1}. A new band due to chlorocyclohexane was observed at 731 cm^{-1}. The time dependence of the catalysed oxidation of cyclohexane shows that the reaction continues for 60 min with 30% conversion of

cyclohexane. Conversion was not observed in the absence of **1** or in the presence of $[Ni^{II}(O_2CCH_3)_2]$ (Figure 3a).

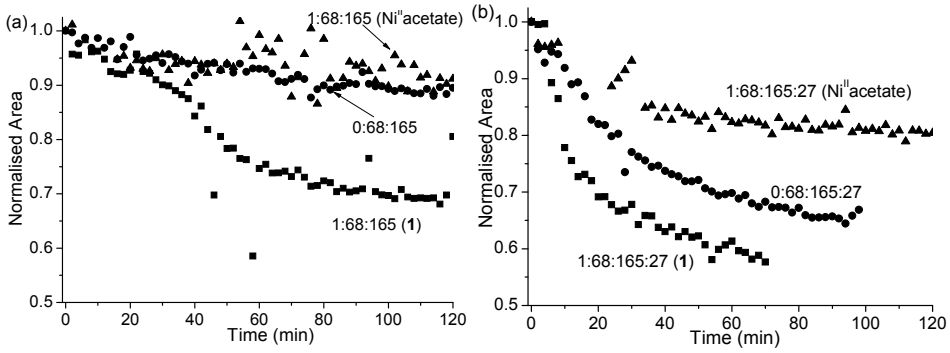

Figure 3 Conversion of cyclohexane to chlorinated products monitored online by Raman spectroscopy (at λ_{exc} 532 nm) using dichlorobenzene as internal standard in the (a) absence and (b) presence of acetic acid. The area under the bands 804 cm^{-1} (cyclohexane) and 662 cm^{-1} (1,2-dichlorobenzene) were used to calculate conversion. See the Table 1 for conditions.

Addition of acetic acid causes the reaction rate to increase and 45% conversion was achieved within 1 h (Figure 3b). It is important to note that, 33% conversion was achieved when acetic acid was added in the absence of **1** over 2 h, albeit with a lower reaction rate.

In the presence of an alkane, with relatively strong C-H bonds, the initially purple solution turned to colourless immediately upon addition of oxidant and then pale orange within a few seconds. After approximately 3 min, a fine black suspension appeared and at the end of the reaction a white solid was obtained. The white solid was identified as $Ni^{II}(OAc)_2$ by Raman spectroscopy. The black solid formed initially could, potentially, be involved in catalysis (*i.e.* nickel nanoparticles), however, it should be noted that although the reaction ceased in terms of conversion of cyclohexane, at ca. 60 min the black solid was still present for a further 30 min indicating that this species is not in fact the active catalyst but rather a catalyst degradation product. Indeed when $Ni^{II}(OAc)_2$ is used instead of **1**, the black particles form also but substrate conversion is not observed.

7.2.3 UV/Vis absorption spectroscopy

In acetonitrile, two CH_3CN ligands are coordinated to the nickel(II) center of **1** in solution. Addition of water to an acetonitrile solution of **1** resulted a red shift in the band at 525 nm to 538 nm and the bands at 321 and 906 nm increased in intensity

(Figure 4a). This is ascribed to the displacement of the CH_3CN ligands with H_2O/OH^- (*vide infra*). Addition of 10.7 eq of NaOCl (~10 μL, 1.66 M in H_2O) to a solution of **1** in acetonitrile resulted in the formation of an orange coloured intermediate (species **A**, which absorbs at 470 nm) over ca. 3 min. The visible absorption spectrum shows a broad increase over the entire spectrum due to scattering from precipitated NaCl and the appearance of absorption bands at λ_{max} 367 and 470 nm, Figure 4b. Over time the two absorption bands decrease in intensity and the solution becomes colourless.

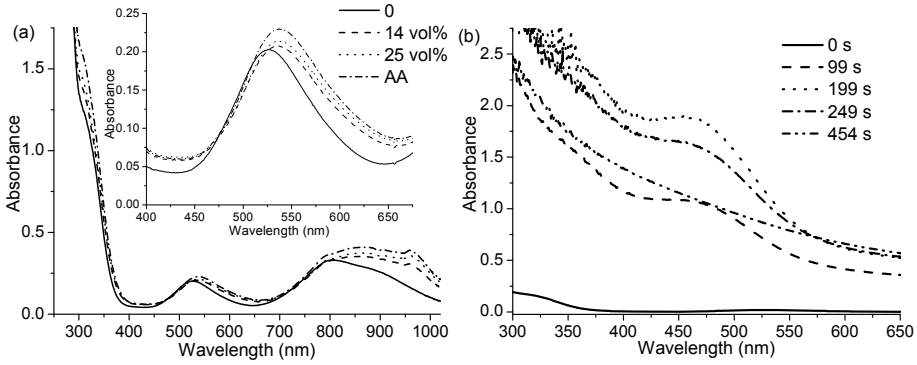

Figure 4 Changes in the UV/Vis absorption spectrum of (a) **1** upon addition of water (14 and 25 vol%) and acetic acid (AA) and (b) **1** (1.55 mM, 1 mL CH_3CN, with stirring) over time with 10.7 eq of NaOCl (~10 μL, 1.66 M in H_2O). The baseline shifts as a result of scattering. # absorption of quartz is observe at 950 nm due to a change in the refractive index upon addition of water.

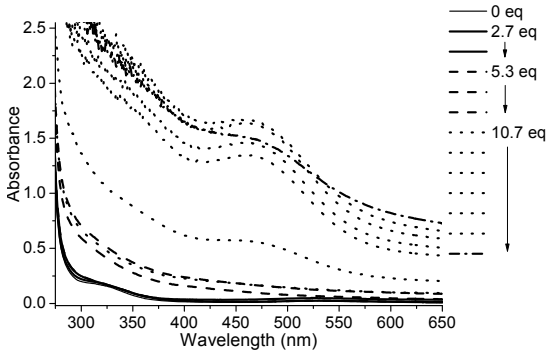

Figure 5 Changes in the UV/Vis absorption spectrum of **1** (1.55 mM, 1 mL CH_3CN, with stirring) over time with 2.7 to 10.7 eq of NaOCl (~10 μL, 1.66 M in H_2O). The baseline shifts as a result of scattering.

The UV/Vis absorption spectrum of **1** changes upon addition of increasing amounts of NaOCl (2.7 to 10.7 eq). The initial weak visible absorbance is replaced by the appearance of an intense absorption in the visible region (Figure 5). In the presence

of acid (*i.e.* acetic acid, triflic acid or sulphuric acid) the intensity of the band is much greater indicating that the formation of the species is proton promoted. Notably, addition of 8.6 eq of triflic acid together with 10.7 eq of NaOCl does not lead to the appearance of a band at 470 nm even after 300 s. The addition of 10.7 more equivalents of NaOCl after 300 s led to a substantial increase in absorbance at 470 nm along with a broad feature at ca. 750 nm. These two absorption bands reach a maximum within one minute, followed by a slow decrease in absorbance.

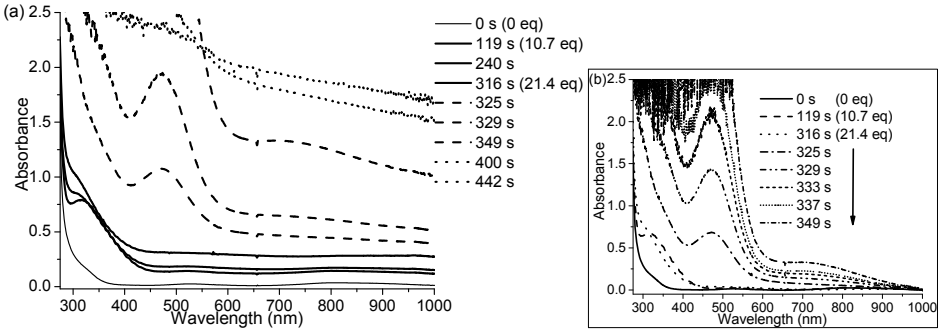

Figure 6 (a) Changes in the UV/Vis absorption spectrum of **1** (1.55 mM) in CH_3CN (with stirring) before and after addition of triflic acid (8.6 eq) and NaOCl (10.7 eq). After 5 min a second 10.7 eq of NaOCl (in water) was added and (b) the baseline corrected spectra. The baseline shifts in (a) are as a result of scattering.

The change from purple to orange occurred also upon addition of aqueous $Ca(OCl)_2$ both in the presence and absence of acetic acid. In the absence of acid, with 17 eq of $Ca(OCl)_2$ the absorbance at 470 nm reached a maximum after 450 s followed by a decrease in absorbance and eventual decolouration of the solution. Addition of a second batch of 17 eq of $Ca(OCl)_2$ to the colourless solution regenerates the absorbance at 470 nm more rapidly than the initial batch had (Figure 7).

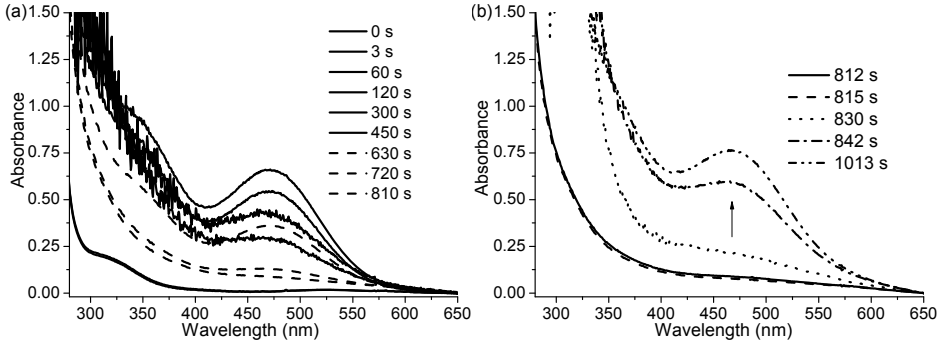

Figure 7 Changes in the UV/Vis absorption spectrum of **1** in acetonitrile upon addition of (a) 17 eq $Ca(OCl)_2$ (with stirring) and (b) at 815 s an additional 17 eq of $Ca(OCl)_2$ was added. Conditions: **1** (1.55 mM, 1 mL CH_3CN), (each 17 eq of $Ca(OCl)_2$ contains 57.6 µL water). Baseline corrected by setting the absorbance at 650 nm to zero.

Addition of 17 eq of $Ca(OCl)_2$ to **1** generates the orange species in the presence of 8.6 eq of acetic acid within 150 s, *i.e.* the formation of the **A** with $Ca(OCl)_2$ is accelerated in the presence of acetic acid. Regeneration of the **A** is possible over several cycles; three cycles are shown in Figure 8a. It should be noted that the band at 470 nm was more intense after the second addition of $Ca(OCl)_2$ compared to the first addition, due to the contribution of attenuation by scattering from particles that are present in the solution, which precludes a detailed kinetic analysis by UV/Vis absorption spectroscopy. Resonance Raman spectroscopy (*vide infra*) suggests, however, that the more rapid increase in absorption is indeed due to faster formation of **A**.

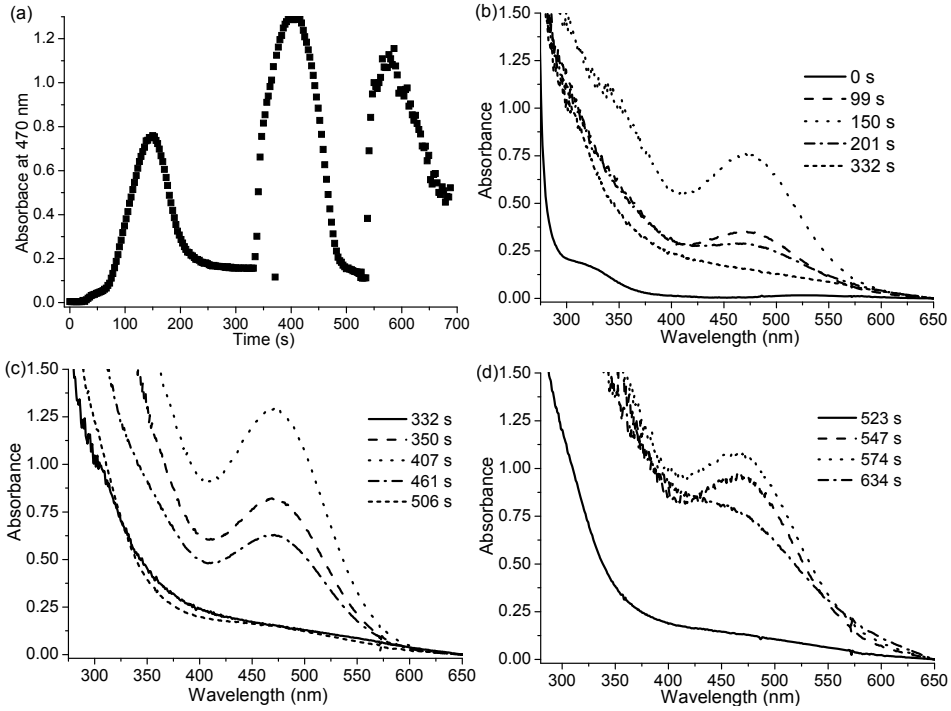

Figure 8 Changes in the UV/Vis absorption spectrum of **1** upon addition of 8.6 eq of acetic acid in acetonitrile and $Ca(OCl)_2$ (with stirring) (a) time dependence of changes in absorbance at 470 nm, (b) with 17 eq $Ca(OCl)_2$, (c) at 332 s a further 17 eq of $Ca(OCl)_2$ were added and (d) at 506 s a further 17 eq of $Ca(OCl)_2$ were added. Conditions: **1** (1.55 mM, 1 mL CH_3CN), (each 17 eq of $Ca(OCl)_2$ contains 57.6 µL water). Spectra are baseline corrected by setting the absorbance at 650 nm to zero.

7.2.3.1 UV/Vis absorption spectroscopy in the presence of substrates

Addition of near stoichiometric amounts of indane (8.6 eq) after addition of NaOCl (10.7 eq) resulted in a complete loss in absorption at 470 nm within 20 s (Figure 9). If the indane (165 eq) is added prior to addition of NaOCl then the absorption band at 470 nm does not appear (Figure 10a).

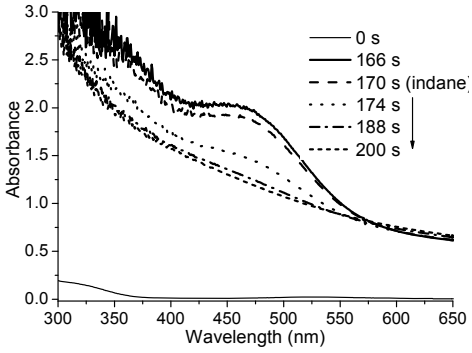

Figure 9 UV/Vis absorption spectrum of **1** in acetonitrile upon addition of 10.7 eq NaOCl (with stirring). After 166 s, 8.6 eq of indane was added. Conditions: **1** (1.55 mM, 1 mL CH_3CN) and 10.7 eq of NaOCl (~10 µL, 1.66 M in H_2O). Baseline shifting is as a result of scattering.

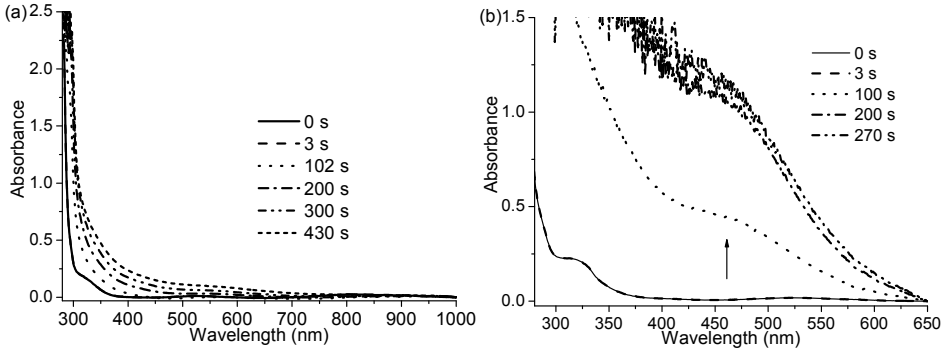

Figure 10 Changes in the UV/Vis absorption spectrum of **1** in acetonitrile with (a) 165 eq of indane followed by 10.7 eq NaOCl and (b) 165 eq of cyclohexane followed by 10.7 eq NaOCl. Conditions: **1** (1.55 mM, 1 mL CH_3CN) and 10.7 eq of NaOCl (~10 µL, 1.66 M in H_2O).

In contrast to indane, addition of cyclohexane (165 eq) either before or after addition of NaOCl has only a modest effect on the appearance of the absorption band at 470 nm. This observation is consistent with its lower reactivity due to its stronger C-H bonds in comparison to indane (Figure 10b).

7.2.4 EPR Spectroscopy

Complex **1** is EPR silent in acetonitrile at 77 K. **A** was generated at 298 K with 10.7 eq of NaOCl and flash frozen to 77 K. The solution shows a signal with $g_{\perp} = 2.13$, and $g_{//} = 2.03$ characteristic of a Ni(III) species.[20] Over time at 298 K the orange colour of the solution becomes yellow and finally colourless. The EPR spectrum of the solution after 10 minutes at 298 K shows similar features, albeit weaker, as that of the initially frozen solution. After several more minutes the solution becomes colourless and the EPR spectrum is silent also (Figure 11 and 12).

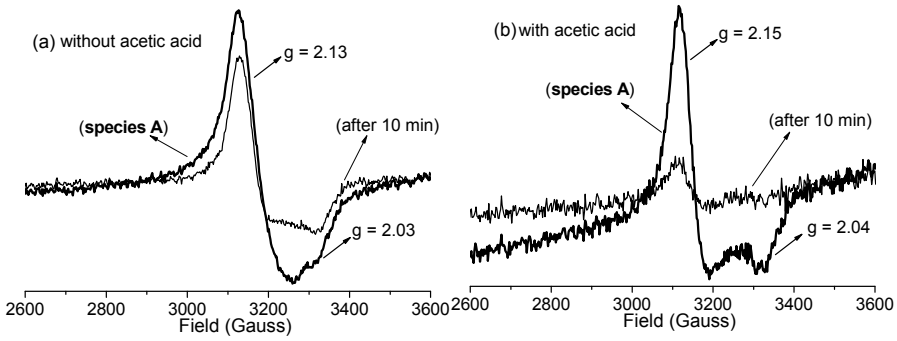

Figure 11 EPR spectra of a solution of **1** (1.55 mM, in CH_3CN) and (a) 10.7 eq NaOCl and (b) 8.6 eq of acetic acid and 21.4 eq NaOCl. Spectra were recorded at 77 K.

Addition of acetic acid was found by UV/Vis absorption spectroscopy to enhance the rate of formation of **A** (*vide supra*). Hence, the effect of acid on the formation of the **A** was explored by EPR spectroscopy. Addition of acetic acid and excess of NaOCl to an acetonitrile solution of **1**, resulted in the appearance of a signal with $g_{\perp} = 2.15$, and $g_{//} = 2.04$ again characteristic of a Ni(III) complex.[20] The perpendicular band was slightly shifted to lower field compared to the signal generated without acid (Figure 12).

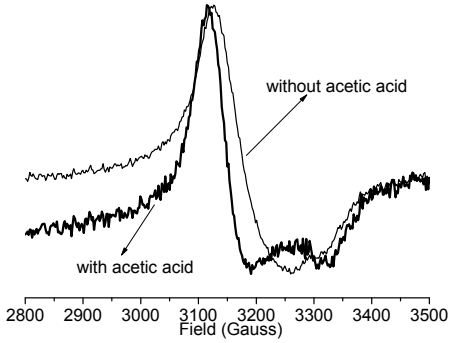

Figure 12 Normalised EPR spectra (Figure of 11a and 11b) of **1** (1.55 mM) in the presence and absence of acetic acid with NaOCl in acetonitrile at 77 K.

The EPR spectra obtained with triflic acid were essentially the same as those obtained with acetic acid (Figure 13). However, the signals observed in the presence of triflic acid were more intense which coincides with the stronger absorbance at 470 nm (Figure 6). This indicates that acid acts as proton source and not a ligand.

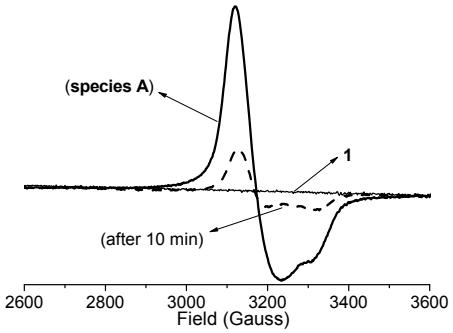

Figure 13 EPR spectra of **1** (3.1 mM) with 8.6 eq of triflic acid and 21.4 eq NaOCl in CH_3CN at 77 K.

EPR spectra of the species generated with $Ca(OCl)_2$ in the presence and absence of acetic acid were essentially the same as those obtained with NaOCl (Figure 14 and 15).

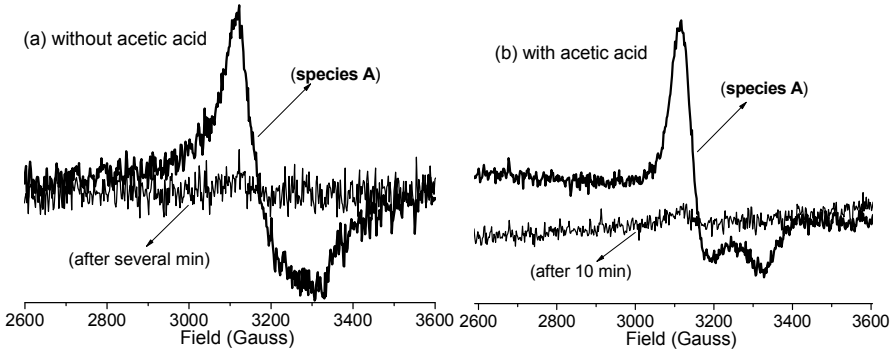

Figure 14 EPR spectra of the solution generated in the reaction between **1** (1.55 mM) and (a) 17 eq $Ca(OCl)_2$ and (b) 8.6 eq of acetic acid (AA) and 17 eq $Ca(OCl)_2$ in CH_3CN at 77 K.

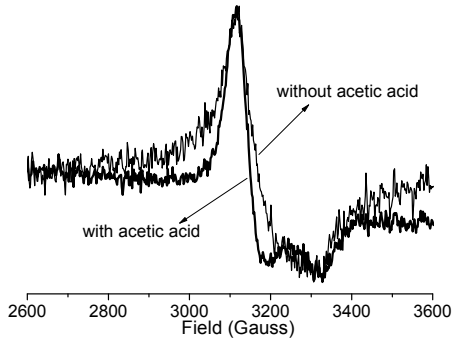

Figure 15 Normalised EPR spectra (Figure of 14a and 14b) of **1** (1.55 mM) in the presence and absence of acetic acid with $Ca(OCl)_2$ in acetonitrile at 77 K.

7.2.5 ^{1}H NMR Spectroscopy

The ^{1}H NMR spectrum of **1** in acetonitrile shows (Figure 16) two broad signals at 49.9 and 47.3 ppm assigned to pyridyl β-protons and a sharp signal at 14.96 ppm assigned to the pyridyl γ-protons by comparison with $[Ni^{II}(TPA)(CH_3CN)(H_2O)]^{2+}$.[21] The signals of the pyridyl α-proton and $PhCH_2$ were not observed.

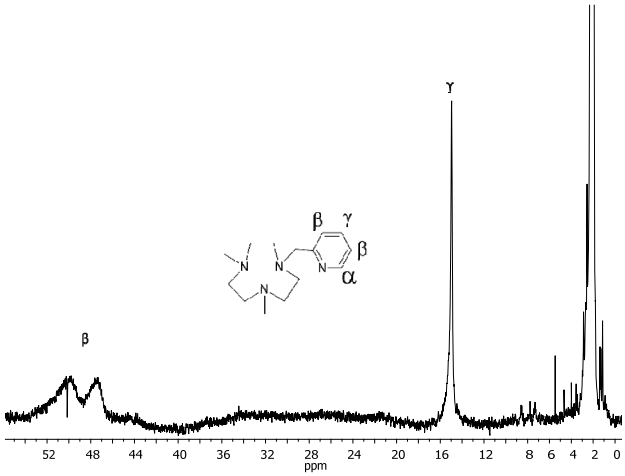

Figure 16 ^{1}H NMR spectrum of **1** (1.55 mM) in CD_3CN at 400 MHz.

The ^{1}H NMR spectra of **1** obtained after addition of 10.7 eq of NaOCl, recorded immediately after appearance of an orange colouration and after 15 minutes, are shown in the Figure 17. The ^{1}H NMR spectra show shifts consistent with substitution of CH_3CN ligands for water. The reaction mixture shows signals at 49.4, 42.8, 15.1, 14.7, 14.47 and 13.37 ppm, and several signals observed between 0-10 ppm. Since Ni(III) complexes would be expected to be NMR silent, the signals are assigned to Ni(II) species, and together with EPR data (*vide infra*) confirms that

in the solution there are several nickel species present in different oxidation states (*e.g.,* Ni^{II} and Ni^{III}).

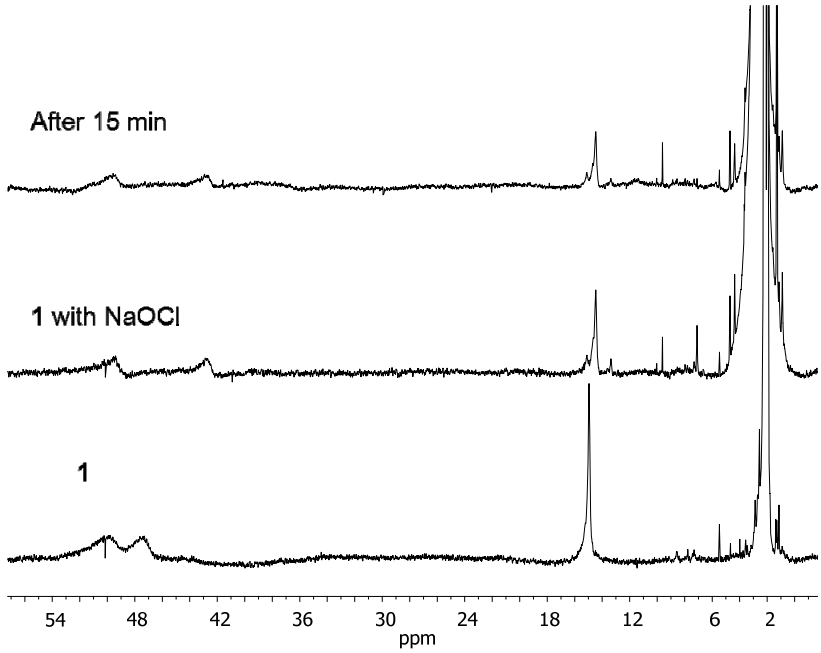

Figure 17 ^{1}H NMR spectrum of **1** (1.55 mM, bottom), and after addition of 10.7 eq of NaOCl (in H_2O, middle) and of the same solution after 15 minutes (top) in CD_3CN at 400 MHz.

The ^{1}H NMR spectra after addition of 17 eq of $Ca(OCl)_2$ to **1**, obtained immediately after appearance of an orange colouration and after 20 minutes are shown in the Figure 18. The spectrum showed signals at 47.64, 42.85 and 14.24 ppm and several signals between 0-6 ppm. The signals at 47.64 and 42.85 were broader and the resonance at 4.42 ppm was not observed in the ^{1}H NMR spectrum of the solution obtained after 20 minutes. The signal 14.24 split into two signals and several additional signals were observed between 7-9 ppm assigned to the non-complexed pyridyl ligand.

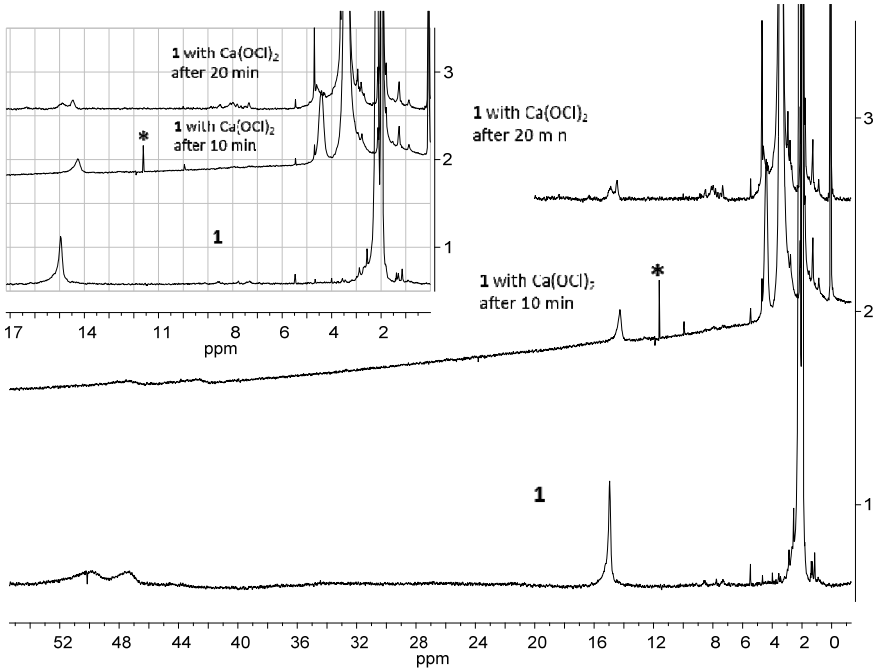

Figure 18 ^{1}H NMR spectrum of **1** and **1** with 17 eq of $Ca(OCl)_2$ (in D_2O) and the same solution after 20 minutes in CD_3CN at 400 MHz. Inset : expansion of 0-17 ppm range. * spectral artefacts.

7.2.6 ESI-MS analysis

ESI-MS is a widely applied technique in the characterisation of first row transition metal complexes allowing for their study under a wide range of solvent conditions.[22] The orange solution generated with 10.7 eq of NaOCl shows several major ions $[(^{H,Me}PyTACN)Ni^{II}(Cl)]^+$ (m/z 341.1), $[(^{H,Me}PyTACN)Ni^{II}(OCl)]^+$ (m/z 357.1) and $[(^{H,Me}PyTACN)Ni^{II}(OTf)]^+$ (m/z 455.09).[23] The peak at m/z 357.1 increased by two mass units when using $Na^{18}OCl$ (10 μL NaOCl in H_2O^{16} + 30 μL H_2O^{18}), which supports its assignment as $[(^{H,Me}PyTACN)Ni^{II}(OCl)]^+$. To avoid interference from the H_2O^{16} present in aq. NaOCl, we carried out analogous experiments using $Ca(OCl)_2$ (solid). The orange solution generated with 17 eq of $Ca(OCl)_2$ (in H_2O) shows major ions $[(^{H,Me}PyTACN)Ni^{II}(OCl)]^+$ (m/z 357.1) and $[(^{H,Me}PyTACN)Ni^{II}(OTf)]^+$ (m/z 455.09). During the reaction the peak at m/z 357.1 decreases relative to the peak at m/z 341.1 $[(^{H,Me}PyTACN)Ni^{II}(Cl)]^+$. The oxygen of $Ca(OCl)_2$ is exchanged with ^{18}O by dissolving it in H_2O^{18}. The peak at m/z 357.1 increased by two mass units when $Ca(^{18}OCl)_2$ was used (Figure 19).

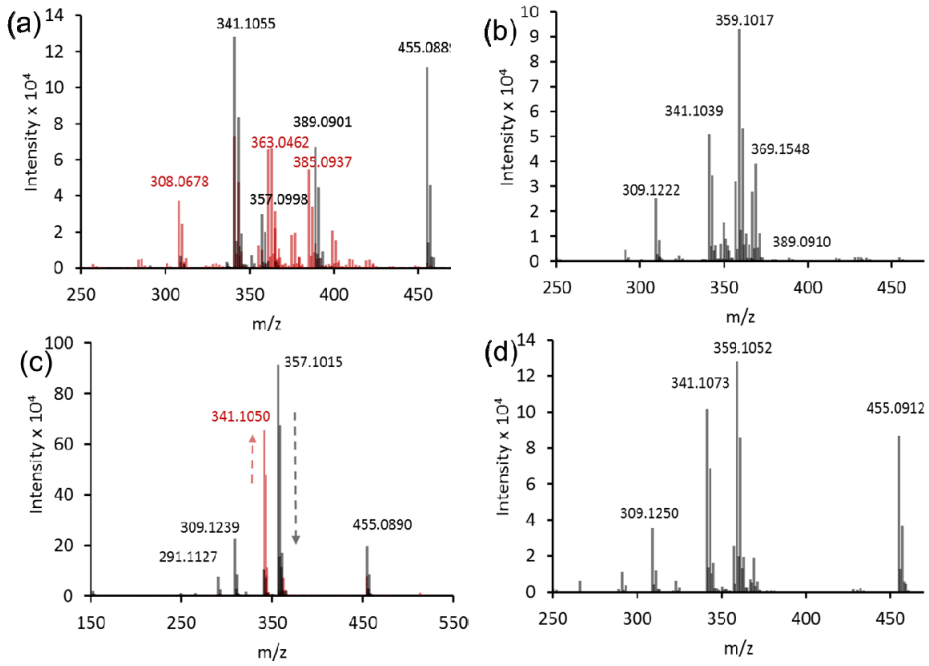

Figure 19 ESI-MS spectra of **1** (1.55 mM) in acetonitrile (a) orange solution generated with 10.7 eq NaOCl, (b) orange solution generated with 10.8 eq NaOCl (10 µL NaOCl in H_2O^{16} + 30 µL H_2O^{18}), (c) orange solution generated with 17 eq $Ca(OCl)_2$ (dissolved in H_2O^{16}) and (d) orange solution generated with 17 eq $Ca(OCl)_2$ (dissolved in H_2O^{18}).

7.2.7 Resonance Raman Spectroscopy

Resonance Raman spectroscopy is a powerful tool both in probing the nature of electronic absorption bands and in characterizing species formed in solution under catalytic conditions. The absence of resonance enhancement of the spectrum of **1** at 785 nm (using the Raman scattering of the triflate bands as an internal reference) is consistent with the assignment of the absorption bands in that region as a metal centred transitions.

The resonance Raman spectrum of the species (**A**), generated upon addition of NaOCl, obtained at λ_{exc} 473 nm shows prominent bands are at 1682, 1618 and 724 cm^{-1} (Figure 20). The band at 1618 cm^{-1} is typical for a pyridyl mode and is indicative of a ligand to metal charge transfer transition at that wavelength[24] (and hence the ligand does not dissociate upon formation of species **A**). The other band at 1682 cm^{-1} is at too high wavenumber shift to be assigned as a pyridyl mode.

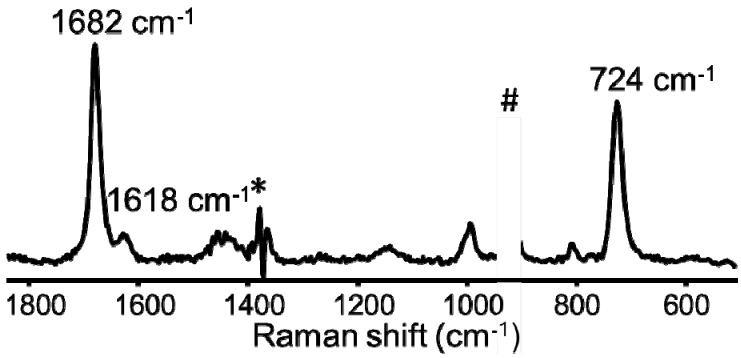

Figure 20 Resonance Raman spectrum at λ_{max} 473 nm of the solution by reaction of **1** (1.55 mM) with NaOCl in acetonitrile. Spectra were obtained with 60 x (3 s) acquisition. * indicates imperfect solvent subtraction. # solvent band distortion covered by white box.

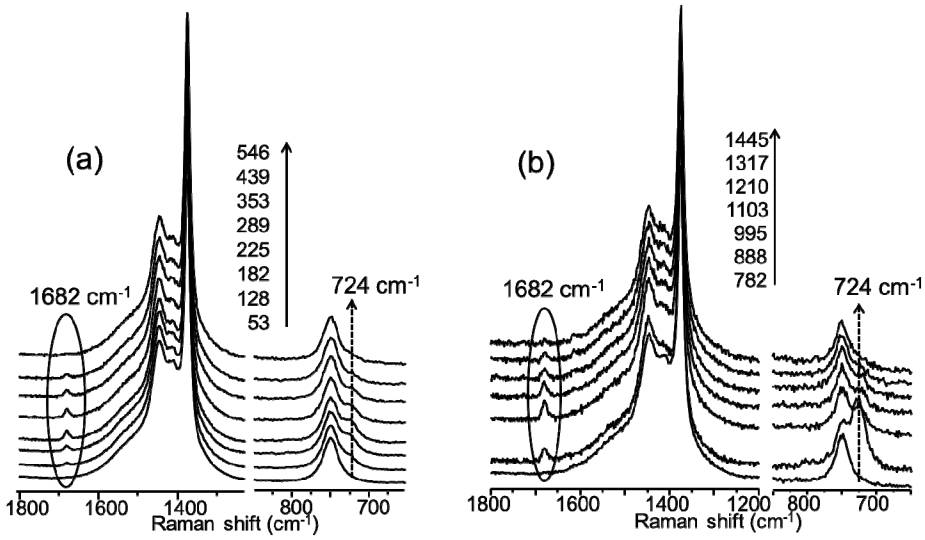

Figure 21 Resonance Raman spectra at λ_{exc} 473 nm of **1** in acetonitrile (with stirring) upon addition of (a) 10.7 eq NaOCl and (b) a second batch addition of NaOCl (10.7 eq) at 782 s. Conditions: **1** (1.55 mM, 1 mL CH_3CN) and 10.7 eq of NaOCl (~10 μL, 1.66 M in H_2O). The legend indicates time in seconds. Spectra were normalised to the acetonitrile bands at 1375 and 756 cm^{-1} and offset for clarity.

Time dependent spectra following the formation of species **A** with 10.7 eq of NaOCl are shown in Figure 21. At the concentrations (1.55 mM) employed for catalysis bands related to the parent Ni(II) complex are too weak to be observed in the Raman spectrum at λ_{exc} 473 nm. In Figure 21a, it can be seen that two bands appear at 1682 and 724 cm^{-1} and reach a maximum intensity at ca. 3-4 min after

addition of NaOCl, and disappear again over time (7-8 min). Complete disappearance of the band at 1682 cm^{-1} was observed after 9 min. These data are consistent with changes observed by UV/Vis absorption spectroscopy specifically the appearance of the absorption band at 470 nm. Addition of a second batch of NaOCl (10.7 eq) resulted in the band at 724 cm^{-1} reaching a maximum intensity after 100 s, but the band at 1682 cm^{-1} does not appear concomitantly suggesting that the 1682 cm^{-1} band arise from a distinct species. Furthermore the band at 1682 cm^{-1} reaches a maximum intensity at ca. 200 s concomitant with a decrease in the intensity of the band at 724 cm^{-1} (Figure 21b). Hence, resonance Raman spectroscopy indicates the involvement of two species (**A** and **B**).

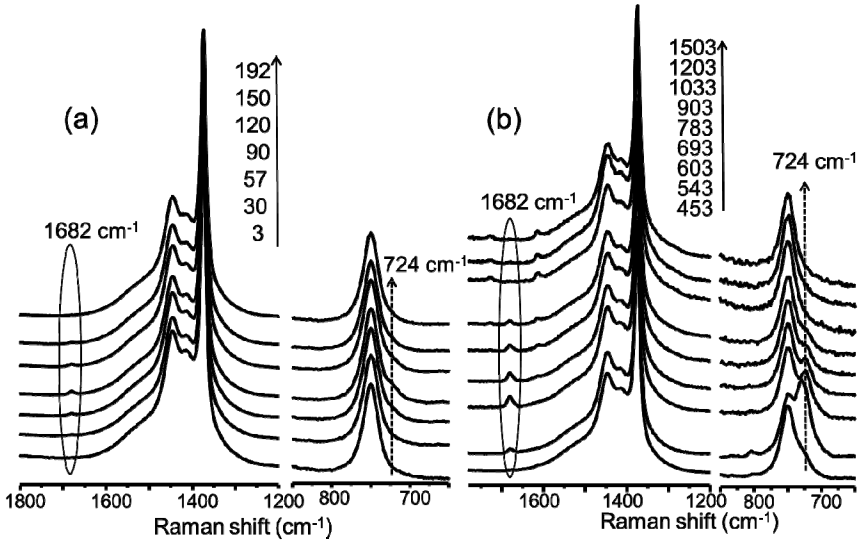

Figure 22 Generation of **A** with **1** in acetonitrile (with stirring) by adding (a) 5.3 eq NaOCl (the scaling of the low wavenumber section is increased for comparison) and (b) second batch addition of NaOCl (10.7 eq) at 400 s monitored by Raman spectroscopy at λ_{exc} 473 nm. Conditions: **1** (1.55 mM, 1 mL CH_3CN) and 4 + 8 eq of NaOCl (in water). In (b) two bands at 1723 and 1622 cm^{-1} are spectral artefacts. Legend indicates time in seconds. Spectra were normalised to the acetonitrile bands at 1375 and 756 cm^{-1}.

UV/Vis absorption spectroscopic analysis indicated that addition of 10.7 eq of NaOCl was necessary to yield substantial absorbance at 470 nm. With 5.3 eq of NaOCl, the bands at 724 and 1682 cm^{-1} were observed, albeit that they are weaker compared to signals generated with 10.7 eq of NaOCl (Figure 22). Addition of a further 10.7 eq of NaOCl to the solution resulted in the band at 724 cm^{-1} reaching a maximum intensity within 100 s, however, the band at 1682 cm^{-1} did not appear concomitantly. It is important to note that the regeneration of **A** from **B** occurs

faster than from **1** initially.

The effect of 8.6 eq of triflic acid or acetic acid on the generation of **A** was examined also. It should be noted that 21.4 eq of NaOCl is needed to generate **A** in the presence of acid.

Addition of 21.4 eq of NaOCl to a solution of **1** containing 8.6 eq of triflic acid leads to the appearance of a Raman band at 724 cm^{-1}, which reaches a maximum intensity within 4-5 min; consistent with UV/Vis absorption spectroscopy (Figure 6). This band decreases in intensity over time. Similar behaviour was observed when employing acetic acid instead of triflic acid. Interestingly, the intensity of the band was higher with triflic acid compared to acetic acid, suggesting that the strength of the acid in acetonitrile plays a role (pK_a of acetic and triflic acids are 23.51 and 0.7 respectively, in acetonitrile).[25] A second batch addition of NaOCl (21.4 eq) regenerates **A** and the band at 724 cm^{-1} reaches a maximum intensity within 1-2 min, suggesting that the resting species (**B**) is not a decomposition product but is instead able to reform the 470 nm absorbing species more rapidly than the initial Ni(II) complex (Figure 23 and 24).

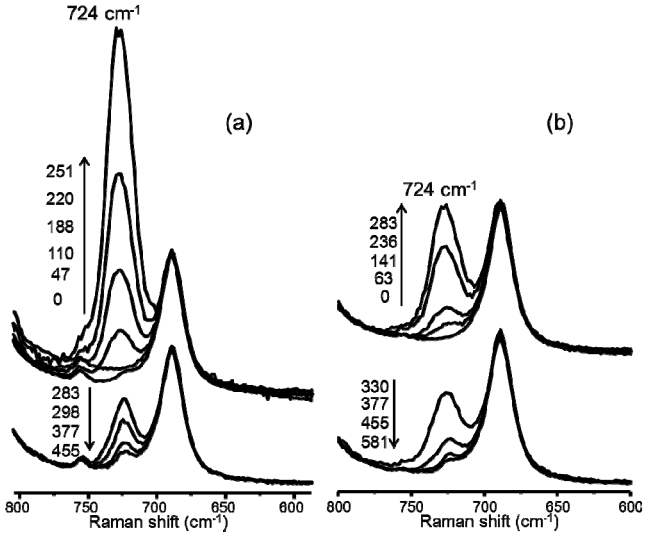

Figure 23 Generation of **A** from **1** in CD_3CN (with stirring) by addition of 21.4 eq of NaOCl (a) in the presence of 8.6 eq of triflic acid and (b) 8.6 eq of acetic acid, monitored by Raman spectroscopy at λ_{exc} 473 nm. Conditions: **1** (1.55 mM, 1 mL CD_3CN), triflic acid (8.6 eq), acetic acid (8.6 eq) and 21.4 eq of NaOCl (~ 20 μL, in water). The legend indicates time in seconds. Spectra were normalised to the CD_3CN band at 686 cm^{-1}.

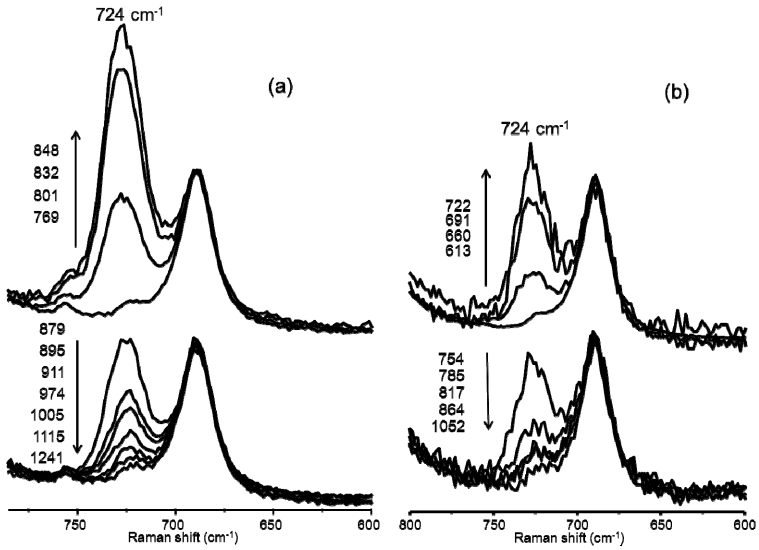

Figure 24 Effect of second batch addition of NaOCl (21.4 eq) to the solution shown in Figure 23 (a) with triflic acid and (b) with acetic acid on the Raman spectrum at λ_{exc} 473 nm. Conditions as in Figure 23. Spectra were normalised to the CD_3CN band at 686 cm^{-1}.

Parallel Raman experiments were carried out with $Ca(OCl)_2$ as oxidant. As with NaOCl, the band at 724 cm^{-1} was also observed in the Raman spectrum of **1** upon reaction $Ca(OCl)_2$ both in the presence and absence of acetic acid (Figure 25). Interestingly, the band at 1682 cm^{-1} was not observed in this case.

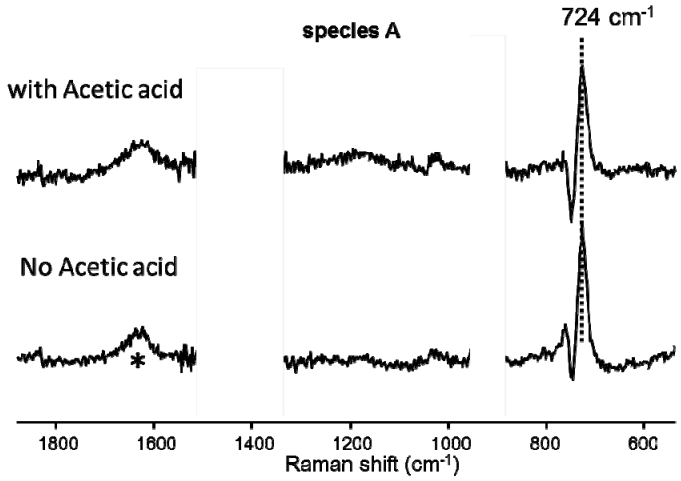

Figure 25 Resonance Raman spectrum at λ_{exc} 473 nm of **1** in CH_3CN (with stirring) after addition of 17 eq of $Ca(OCl)_2$ in the presence and absence of 8.6 eq of acetic acid. Conditions **1** (1.55 mM, 1 mL CH_3CN), 17 eq of $Ca(OCl)_2$ (in 60 µL of water). * Spectra are solvent subtracted.

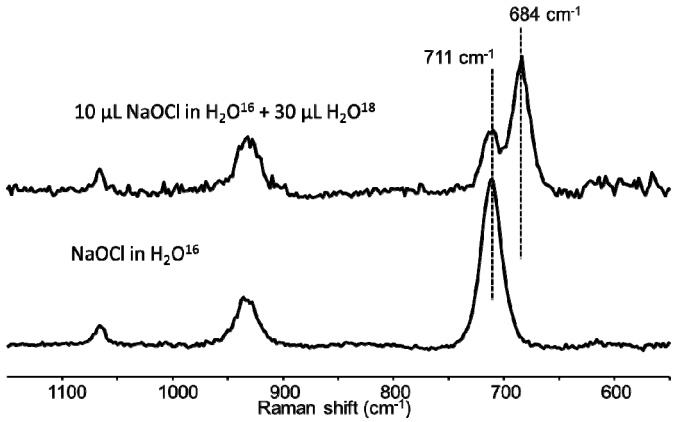

Figure 26 Raman spectra of NaOCl in H_2O^{16} and NaOCl diluted in H_2O^{18} (10 µL NaOCl in H_2O^{16}+ 30 µL H_2O^{18}) at λ_{exc} 785 nm.

The O-Cl stretching band of NaOCl was observed at 711 cm^{-1}. ^{18}O-labelled NaOCl was prepared by mixing 10 µL NaOCl (in H_2O^{16}) with 30 µL of H_2O^{18} (*i.e.* 1:3 H_2O^{16} and H_2O^{18}). Exchange of oxygen was confirmed by Raman spectroscopy (Figure 26). A statistical distribution of 1:3 was observed between the bands 711 cm^{-1} and 684 cm^{-1}. The observed shift 27 cm^{-1} is in agreement with the calculated shift based on the two atom approximation of O-Cl (28 cm^{-1}).

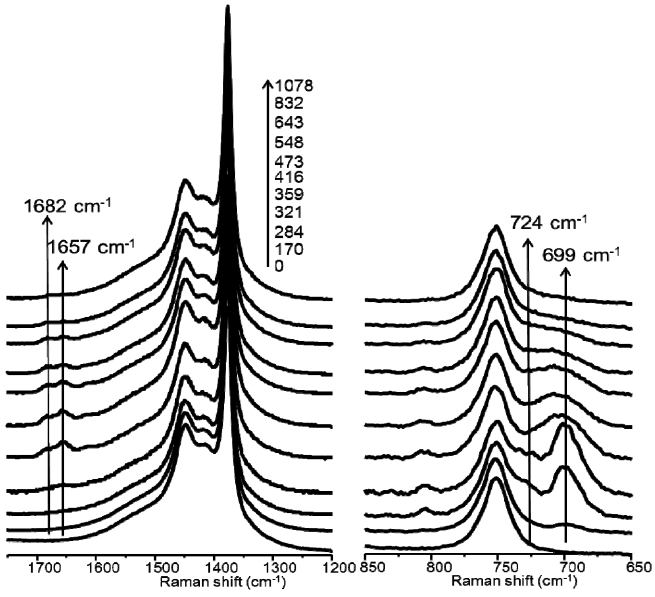

Figure 27 Reaction of **1** (1.55 mM) in 1 mL of acetonitrile with 10.7 eq of NaOCl (40 µL; 10 µL NaOCl in H_2O^{16}+ 30 µL H_2O^{18}), monitored by Raman spectroscopy at λ_{exc} 473 nm. The legend indicates time in seconds. Spectra were normalised to the acetonitrile bands at 1375 and 756 cm^{-1}.

A new band at 699 cm^{-1} along with the band at 724 cm^{-1} was observed when NaOCl diluted in H_2O^{18} (*i.e.* 1:3 H_2O^{16} and H_2O^{18}) was employed. The ~ 1:3 ratio observed between the bands is consistent with the expected statistical ratio. A shift of 25 cm^{-1} was observed upon O^{18} labelling (Figure 27). To assign this mode as either a Ni-O or O-Cl stretch, the 724 cm^{-1} band should shift by 32 or 28 cm^{-1}, respectively, according to the Hooke's law using the two atom approximation. Notably, the band at 1682 shifts to 1655 cm^{-1}, *i.e.* a 25 cm^{-1} also. NaOBr was employed to assist in the assignment of bands at 724 and 1682 cm^{-1}. Two intense bands at 728 and 1679 cm^{-1} were observed in the Raman spectrum upon addition of NaOBr (Figure 28). These shifts of 4 and 3 cm^{-1}, respectively, are negligible especially considering that the introduction of bromine should shift these bands by 50-60 cm^{-1}, and hence the band at 728 cm^{-1} is not a Ni-**O-Br** stretch. The Raman band at 724 cm^{-1} is close to that of a Fe^{III}-O (690-610 cm^{-1}).[26] Based on the ^{18}O labelling and bromine labelling data, we assigned the 724 cm^{-1} band as a Ni-O stretch. The ^{18}O isotope shift of band at 1682 cm^{-1} is not consistent with a O-H stretch of a Ni^{II}-O-H (species **B**).

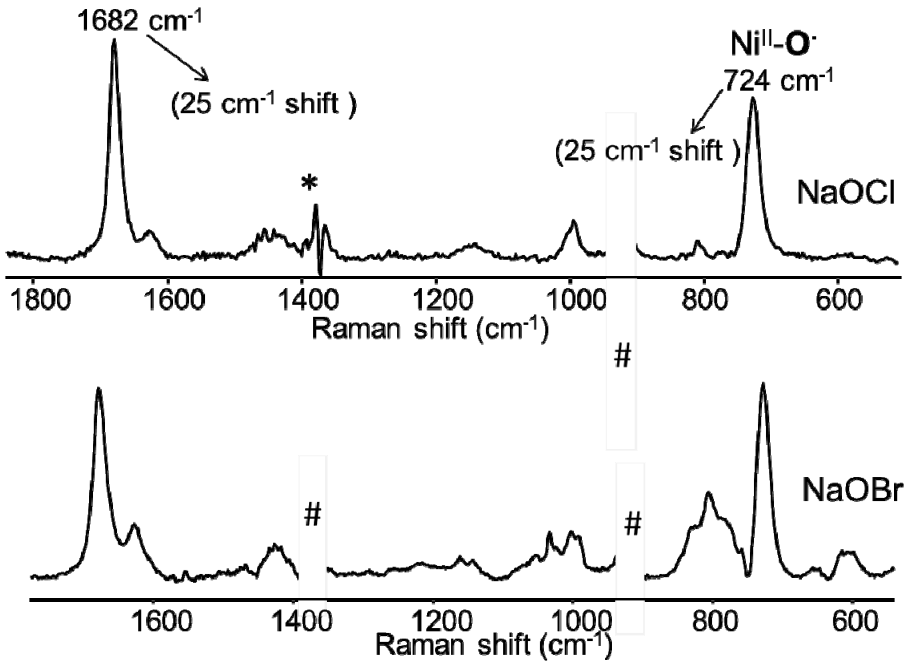

Figure 28 Resonance Raman spectrum of **A** generated in the reaction between **1** (1.66 mM, 1 mL CH_3CN) with acetic acid (8.6 eq) and NaOBr (10.7 eq, 20 μL) in acetonitrile at λ_{max} 473 nm. # Artefacts due to solvent subtraction were masked with white box.

Furthermore in the Raman spectrum of **A**, bands related to either of O-Cl or O-Br were not evident, suggesting that **A** does not contain a Ni^{II}-OCl moiety. Hence, our assignment of **A** is a Ni^{II}-$O^{\cdot}$ or a Ni^{III}-OH.

Evidence for a Ni^{II}-OCl species was not obtained by resonance Raman spectroscopy such as that observed by ESI-MS (*vide supra*). This lack of observation by Raman spectroscopy may be due to the lack of resonance enhancement of the Raman scattering of Ni^{II}-OCl species at λ_{exc} 473 nm, *i.e.* absence of evidence is not evidence of absence.

7.3 Summary and mechanistic considerations

7.3.1 Reactions in the absence of a Ni(II) catalyst

It is important to note that chlorination of substrates is observed both in the absence and presence of the Ni(II) complex (**1**), albeit at lower rates and with lower conversions in the former case. This is not surprising, since acid catalysed reactions with NaOCl are well described in the literature.[27] In the absence of **1** and in the presence of acetic acid the reaction is likely to proceed through a radical pathway involving hypochlorous acid, which is formed *in situ* upon addition of sodium hypochlorite to the acetic acid. The proposed mechanism for the acid catalysed reaction is depicted in Scheme 2.[27]

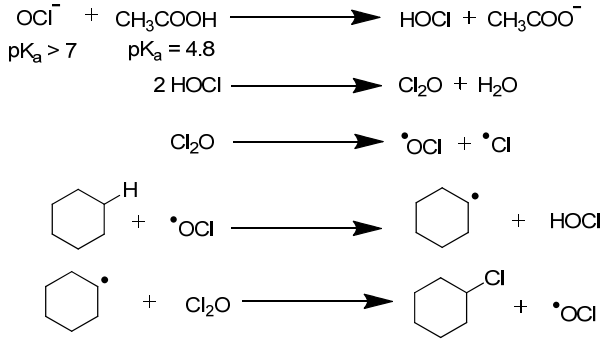

Scheme 2 Proposed mechanism for acid catalysed reaction.[27]

Protonation of hypochlorite in the presence of acetic acid generates hypochlorous acid. Chloroxyl radicals can be generated from hypochlorous acid, which is able to abstract a hydrogen from cyclohexane and generate alkyl radicals. These alkyl radicals further react with Cl_2O, to produce chlorinated products and regenerate the chloroxyl radicals. Notably, in the presence of $[Ni^{II}(O_2CCH_3)_2]$, the acid catalysed reaction is in fact retarded and lower conversion is observed possible due to quenching of radicals formed.

7.3.2 Catalysis in the presence of 1

Raman spectroscopy confirms that complex **1** retains the CH_3CN ligand in acetonitrile solution, and its octahedral structure (Figure 1).[17,18] Addition of water to an acetonitrile solution of **1**, leads to the displacement of CH_3CN ligands with either aqua/hydroxo ligand albeit with the overall structure of the complex being retained (Figure 4).

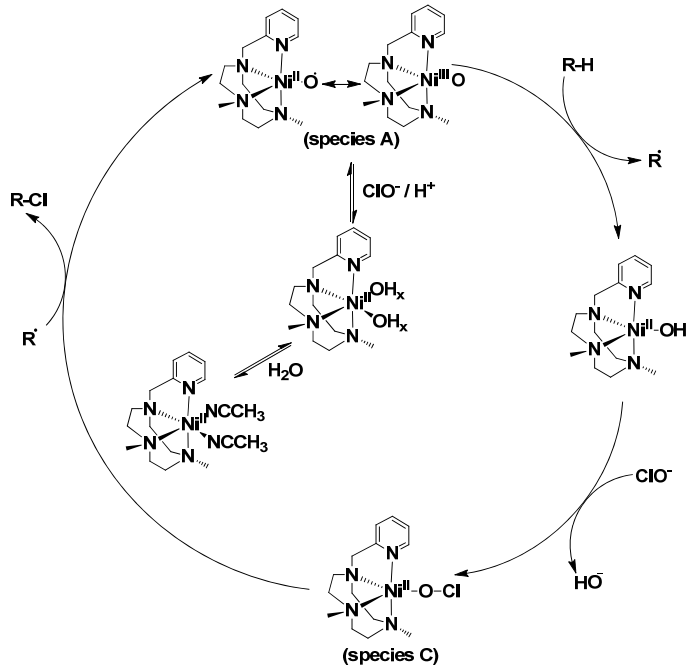

Scheme 3 Proposed mechanism for C-H chlorination reaction under ambient atmosphere.

It is apparent from UV/Vis absorption spectroscopy that addition of aqueous NaOCl to **1** in acetonitrile results in the formation of a species **A** that is orange in colour and potentially reacts with substrates. That 10 eq of oxidant is needed to generate the species suggestive that the initial step may be rate limiting (*i.e.* formation of a N^{II}-OCl species **C**). Species **A** is likely to be of the type Ni^{II}-$O^{\cdot}$ with a ^{18}O sensitive Raman band at 724 cm^{-1} and characteristic EPR signals. The requirement of 10 eq of aqueous NaOCl is attributed to generate the $[(L)Ni^{II}(OH_x)_2]$ (where x = 1 or 2), which then reacts with the oxidant. This Ni^{II}-$O^{\cdot}$ (**A**) species is responsible for abstraction of a hydrogen from the alkane substrate and forms alkyl radicals and a Ni^{II}-OH species, since conversion is observed concomitant with the presence of **A**.[28] Indeed species **A** is present at much lower levels in the presence of substrates than

in their absence. The formation of the halogenated product requires that the [(L)Ni^{II}-OCl] complex species **C** (observed by ESI-MS) reacts with the alkyl radical, and the species Ni^{II}-$O^{\cdot}$ is restored.[29] After several turnovers (ca. 20) nickel acetate (in the presence of acetic acid) and nickel oxide (in the absence of acid) were observed.

7.4 Conclusions

In conclusion, we report a selective catalytic system for chlorination of alkanes with Ni(^{H,Me}PyTACN) complex. The intermediates Ni^{II}-$O^{\cdot}$ (**A**) and Ni^{II}-OCl (**C**) were characterised by UV/Vis absorption, EPR and resonance Raman spectroscopy and ESI-MS, respectively. The Raman band at 724 cm^{-1} assigned as a Ni-O stretch of species **A**. To the best of our knowledge, this is the first spectroscopic evidence for the involvement of Ni^{II}-$O^{\cdot}$ and Ni^{II}-OCl species in catalysis. Importantly we can exclude that the black particulate species formed is involved in the catalytic halogenation reactions.

7.5 Experimental section

The ligand ^{H,Me}PyTACN was available from earlier studies.[16]

7.5.1 Physical Methods

For details of UV/Vis absorption, ^{1}H NMR, Raman, resonance Raman, FTIR, EPR and Electrochemical measurements, see chapter 2. For details of ESI-MS measurements, see chapter 6. Crystals suitable for X-ray crystallography were obtained by slow diffusion of ether into an acetonitrile solution of **1**. These crystals of **1** used for room temperature (300(2) K) X-ray structure determination. The measurement was carried out on a *BRUKER SMART APEX CCD* diffractometer using graphite-monochromated Mo *K*α radiation (λ = 0.71073 Å) from an X-ray Tube. The measurements were made in the range 2.04 to 28.69° for θ. Full-sphere data collection was carried out with ω and φ scans. A total of 43320 reflections were collected of which 7175 [R(int) = 0.0528] were unique. Programs used: data collection, Smart; data reduction, Saint+; absorption correction, SADABS. Structure solution and refinement was done using SHELXTL Version 6.14 (Bruker AXS 2000-2003). The structure was solved by direct methods and refined by full-matrix least-squares methods on F^2. The non-hydrogen atoms were refined anisotropically. The H-atoms were placed in geometrically optimized positions and forced to ride on the atom to which they are attached. (Final R indices [I>2sigma(I)] -- R1 = 0.0436, wR2 = 0.1090; R indices (all data) -- R1 = 0.0610, wR2 = 0.1194 and Absolute structure parameter 0.092(14).

7.5.2 Synthesis

[Ni(^{H,Me}PyTACN)(CH_3CN)(OTf)](OTf) (1). A solution of $Ni(CH_3CN)_6(OTf)_2$ (242.7 mg, 0.40 mmol) in anhydrous THF (1 mL) was added drop wise to a vigorously stirred solution

of ^{H,Me}PyTacn (99.8 mg, 0.40 mmol) in CH_2Cl_2 (1 mL). After two hours, the solution becomes cloudy and a pale violet precipitate appears. After stirring for 2 h the solution was filtered off and the resultant solid dried under vacuum. This solid was dissolved in CH_3CN and slow diethyl ether diffusion affords 102 mg of intense violet crystals (0.26 mmol, 66%). The sampler for elemental analysis was crushed and kept under vacuum for 12 h prior the analysis changing the colour to pale violet. Anal. Calcd. for (**1Ni**+CH_3CN) $C_{18}H_{27}F_6N_5NiO_6S_2$: C, 33.45; H, 4.21; N, 10.84; S, 9.92 %. Found: C, 33.74; H, 3.97; N, 10.69; S, 10.09 ESI-MS (m/z): 455.1 $[M\text{-}OTf]^+$ (100%), 153.0 $[M]^{2+}$ (16%).

7.5.3 Catalysis

63 µL NaOCl (104.9 µmol, 10-15 active chlorine NaOCl) in water was added to a stirred solution of **1** (1.55 µmol), alkane (255.4 µmol,) in 1 mL acetonitrile in a 10 mL sealed vial. The resulted solution was stirred vigorously for 2 h. Reactions were run at room temperature after 2 h the internal standard (biphenyl) was added and the solution was filtered through a basic alumina plug, which was subsequently rinsed with 3 mL of dichloromethane. Samples were filtered over a short silica plug and analysed by GC on an Agilent 6890 instrument equipped with a HP-1 dimethylpolysiloxane column (for KIE determination a CPWax25 column). Products were quantified with respect to the biphenyl internal standard.

7.6 Acknowledgements

Prof. M. Costas, Dr. A. Company, Dr. J. Lloret-Fillol, Dr. L. Gómez and Z. Codolà are greatly acknowledged for collaboration and useful discussions.

7.7 References

(1) (a) J. E. Bäckvall, Ed., *Modern Oxidation Methods*, Wiley-VCH, **2004**; (b) T. Punniyamurthy, S. Velusamy, J. Iqbal, *Chem. Rev.*, **2005**, *105*, 2329-2363; (c) M. Costas, M. P. Mehn, M. P. Jensen, L. Que, Jr., *Chem. Rev.*, **2004**, *104*, 939-986.

(2) (a) Y. Hitomi, K. Arakawa, T. Funabiki, M. Kodera, *Angew. Chem. Int. Ed.*, **2012**, *51*, 3448-3452; (b) G. Roelfes, M. Lubben, K. Chen, R. Y. N. Ho, A. Meetsma, S. Genseberger, R. M. Hermant, R. Hage, S. K. Mandal, V. G. Young, Jr., Y. Zang, H. Kooijman, A. L. Spek, L. Que, Jr., B. L. Feringa, *Inorg. Chem.,* **1999**, *38,* 1929-1936.

(3) F. Li, K. K. Meier, M. A. Cranswick, M. Chakrabarti, K. M. Van Heuvelen, E. Münck, L. Que, Jr., *J. Am. Chem. Soc.,* **2011**, *133*, 7256-7259.

(4) (a) A. Karlsson, J. V. Parales, R. E. Parales, D. T. Gibson, H. Eklund, S. Ramaswamy, *Science,* **2003**, *299*, 1039-1042; (b) L. V. Liu, C. B. Bell, S. D. Wong, S. A. Wilson, Y. Kwak, M. S. Chow, J. Y. Zhao, K. O. Hodgson, B. Hedman, E. I. Solomon, *Proc. Natl. Acad. Sci. U.S.A.*, **2010**, *107*, 22419-22424.

(5) A. Lennartson, C. J. McKenzie, *Angew. Chem. Int. Ed.,* **2012**, *51*, 6767-6770.

(6) Z. Cong, S. Yanagisawa, T. Kurahashi, T. Ogura, S. Nakashima, H. Fujii, *J. Am. Chem. Soc.*, **2012**, *134*, 20617-20620.

(7) L. C. Blasiak, C. L. Drennan, *Acc. Chem. Res.*, **2009**, *45*, 147-155.

(8) (a) A. S. Borovik, *Chem. Soc. Rev*., **2011**, *40*, 1870-1874; (b) M. Costas, K. Chen, L. Que, Jr., *Coord. Chem. Rev.*, **2000**, *200-202*, 517-544; (c) T. Punniyamurthy, S. Velusamy, J. Iqbal, *Chem. Rev.*, **2005**, *105*, 2329-2363.
(9) (a) A. Sorokin, A. Robert, B. Meunier, *J. Am. Chem. Soc.*, **1993***, 115,* 7293-7299; (b) W. Liu, J. T. Groves, *J. Am. Chem. Soc.,* **2010**, *132*, 12847-12849.
(10) J. M. Grill, J. W. Ogle, S. A. Miller, *J. Org. Chem.,* **2006**, *71*, 9291-9296; (b) C. Querci, S. Strologo, M. Ricci, *Tetrahedron Lett.*, **1990**, *31*, 6577-6580.
(11) (a) H. Yoon, C. J. Burrows, *J. Am. Chem. Soc.,* **1988,** *110,* 4087-4089; (b) H. Yoon, T. R. Wagler, K. J. O'Connor, C. J. Burrows, *J. Am. Chem.* Soc., **1990,** *112,* 4570-4571.
(12) T. Nagataki, Y. Tachi, S. Itoh, *Chem. Commun.*, **2006**, 4016-4018.
(13) F. F. Pfaff, F. Heims, S. Kundu, S. Mebs, K. Ray, *Chem. Commun.,* **2012**, *48*, 3730-3732.
(14) J. R. Winkler, H. B. Gray, *Struct. Bonding*, **2011**, *142*, 17-28.
(15) R. H. Holm, *Chem. Rev.*, **1987**, *87*, 1401-1449.
(16) A. Company, L. Gómez, M. Güell, X. Ribas, J. -M. Luis, L. Que, Jr., M. Costas, *J. Am. Chem. Soc.*, **2007**, *129*, 15766-15767.
(17) T. Nagataki, K. Ishii, Y. Tachi, S. Itoh, *Dalton Trans.*, **2007**, 1120-1128.
(18) T. R. Holman, M. P. Hendrich, L. Que, Jr., *Inorg. Chem.*, **1992**, *31*, 937-939.
(19) H. J. H. Fenton, *J. Chem. Soc.*, **1894**, *65*, 899-910.
(20) J. Cho, H. Y. Kang, L. V. Liu, R. Sarangi, E. I. Solomon, W. Nam, *Chem. Sci.*, **2013**, *4*, 1502-1508.
(21) E. Szajna, P. Dobrowolski, A. L. Fuller, A. M. Arif, L. M. Berreau, *Inorg. Chem.,* **2004**, *43*, 3988-3997.
(22) (a) J. B. Fenn, M. Mann, C. K. Meng, S. F. Wong, C. M. Whitehouse, *Mass Spectrom. Rev.*, **1990**, *9*, 37-70; (b) J. H. Kim, Y. H. Dong, E. Larka, L. Que, Jr., *Inorg. Chem.*, **1996**, *35*, 2369-2372; (c) D. Feichtinger, D. Plattner, *Angew. Chem. Int. Ed. Engl.*, **1997**, *36*, 1718-1719; (d) D. Feichtinger, D. Plattner, *J. Chem. Soc., Perkin Trans.*, **2000**, *2*, 1023-1028; (e) B. C. Gilbert, J. R. Lindsay Smith, M. S. Newton, J. Oakes, R. Pons i Prats, *Org. Biomol. Chem.*, **2003**, *1*, 1568-1577; (f) O. Bortolini, V. Conte, *Mass Spectrom. Rev.*, **2006**, *25*, 724-740.
(23) Chlorido (Cl^-) and triflate (^-OTf) can also be act as ligands (see ESI-MS section). The Ni(II) species observed in NMR spectroscopy can be any of these complexes.
(24) A. Draksharapu, Q. Li, H. Logtenberg, T. A. van den Berg, A. Meetsma, J. S. Killeen, B. L. Feringa, R. Hage, G. Roelfes, W. R. Browne, *Inorg. Chem*., **2012**, *51,* 900-913.
(25) E. Raamat, K. Kaupmees, G. Ovsjannikov, A. Trummal, A. Kütt, J. Saame, I. Koppel, I. Kaljurand, L. Lipping, T. Rodima, V. Pihl, I. A. Koppel, I. Leit, *J. Phys. Org. Chem.*, **2013**, 6, 162-170.
(26) J. J. McGarvey, A. Draksharapu, W. R. Browne, *Special Periodic Reports*, **2013**, *44*, 68-94.
(27) (a) H. E. Fonouni, S. Krishnan, D. G. Kuhn, G. A. Hamilton, *J. Am. Chem. Soc.*, **1983**, *105*, 7672-7676; (b) E. Raamat, K. Kaupmees, G. Ovsjannikov, A. Trummal, A. Kütt, J. Saame, I. Koppel, I. Kaljurand, L. Lipping, T. Rodima, V. Pihl, I. A. Koppel, I. Leito, *J. Phys. Org. Chem.*, **2013**, *26*, 162-170.
(28) H. Yoon, T. R. Wagler, K. J. O'Connor, C. J. Burrows, *J. Am. Chem. Soc*., **1990**, *12*, 4570-4571.
(29) W. Liu, J. T. Groves, *J. Am. Chem. Soc.*, **2010**, *132*, 12847-12849.